VERTICAL PROPAGATION OF GRAVITY WAVES DETERMINED FROM ZENITH OBSERVATIONS OF AIRGLOW

E. R. Reisin and J. Scheer

published in Advances in Space Research 27(10), 1743-1748, 2001.

VERTICAL PROPAGATION OF GRAVITY WAVES DETERMINED FROM ZENITH OBSERVATIONS OF AIRGLOW

E. R. Reisin and J. Scheer [1]

[1] *Instituto de Astronomía y Física del Espacio, CONICET, Ciudad Universitaria, 1428 Buenos Aires, Argentina*

ABSTRACT

From our growing data base of OH and O_2 airglow intensity and temperature measurements at lower mid-latitudes, gravity wave information has been extracted by time series spectral analysis. According to existing theories, the amplitude and phase relationships between intensities and rotational temperatures for a given airglow emission contain information about vertical wave propagation. A wide but clearly non-random distribution of phase shifts between intensity and temperature is observed. Cases of 180°, often cited in the literature, are definitely exceptions, here. For observed periods between about ten minutes and three hours, 30% of the waves at 95 km, and 40% at 87 km propagate downward. This signals the importance of wave reflection in the mesopause region.

INTRODUCTION

There are many recent studies about gravity wave characteristics, in the mesopause region. Only some techniques can derive all the intrinsic wave parameters, simultaneously. From the horizontal wave propagation and wind information, also the vertical wavelength λ_z can be derived via the dispersion relation, but not the sense of vertical propagation. Radar and lidar techniques can directly determine λ_z, including its sign (see, e.g., the radar results by Gavrilov et al., 1997), but are limited to $\lambda_z \lesssim 20$ km. Therefore, combining different techniques, like radar and airglow observations, can be expected to give more complete information (e.g., Takahashi et al., 1999).

It is therefore remarkable that the kind of optical zenith observations as discussed here can not only derive λ_z but also distinguish between upward and downward phase propagation. This is due to the fact supported by some theories (Hines and Tarasick, 1987; Swenson and Gardner, 1998) that the sign of the phase difference between gravity-wave induced brightness and rotational temperature oscillations of the same airglow emission depends directly on the sense of vertical propagation (for other recent theoretical results, see Makhlouf et al., 1998; for more references, Reisin and Scheer 1996a).

Thanks to the large base of airglow data from our instrument, that has already surpassed 700 nights of observation, a reliable statistical analysis of vertical propagation characteristics has been possible. These results are obtained independently for two different airglow emissions, yielding interesting information about how these characteristics change with height, in the mesopause region.

The present paper is limited to observed periods between 1000 and 10000 seconds (17 to 167 minutes). The lower period limit (still well above the Nyquist period of 2.7 min) is to safely avoid certain (unpublished) systematic biasses due to a combination of low-pass filtering effects related to the sequential spectral sampling. The upper limit (≈ 3 h) is meant to discriminate against waves in the tidal period range discussed elsewhere (Reisin and Scheer, 1996a). In the tidal case, the identification of the same wave simultaneously in both emission layers is often possible (which was used to validate the technique). Here, this identification is not generally possible, because of differential Doppler shift due to wind shear. Therefore, there is no alternative to extracting λ_z from Hines' and Tarasick's relation (see below), unless background winds and

horizontal propagation characteristics are known.

DATA AND ANALYSIS TECHNIQUE

The data, OH(6-2) and O_2b(0-1) band intensities and temperatures, have been acquired with the same tilting filter spectrometer used in all our previous work. Since 1997, the instrument operates with a new filter, and under PC control which permits unattended operation and time resolution improved from 104 s, to 81 s, now (see also Scheer and Reisin, 2001). The data used here comprise the observations during campaigns from El Leoncito (31.8°S, 69.2°W)in 1987 and 1992, and from El Arenosillo (Spain; 37.1°N, 6.7°W), in 1990, and since August 1997, the nearly continuous measurements from El Leoncito (Scheer and Reisin, 2000). In addition, 60 more recent nights between October 1999 and mid-February 2000 are also included here. The present analysis focusses on the large and more homogeneous part of the data corresponding to 1997 - 2000 that consists of 444 nights and about 150,000 sets of observations, and the older data are used for comparison.

We do not normally see monochromatic gravity waves. At any rate, there are considerable differences between the characteristics of (high amplitude) quasi-monochromatic waves and the majority of small amplitude waves, as shown by Walterscheid et al. (1999). So, in order to detect individual wave signatures, time series spectral analysis is performed for temperature and intensity data. A periodogram technique is used to extract the principal spectral components, without, of course, any restrictions on periods. Peaks from the intensity and temperature spectra with coincident period are then considered as a potential wave signature, and subjected to further analysis.

A periodogram method for non-equally-spaced data is used. It has been employed in several previous studies (e.g., Scheer et al., 1994). The precision of the frequency determination is much better than the equivalent Fourier spacing. The periodogram is computed iteratively after subtracting from the data the sinusoid corresponding to the spectral component that represents maximum data variance. This method efficiently removes sidelobe effects. The periodogram is computed over the complete frequency range between zero and the cutoff frequency defined by the minimum data spacing. Therefore, the previous removal of any linear and sinusoidal trends is not necessary. Since the spectral components are generated in the order of importance, the iteration can be aborted after the principal components are obtained. To improve wave detection in view of the limited duration of wave events, 3-hour data windows (with 50% overlap) are used. Several rather strict selection criteria are applied automatically to insure 75% completeness and homogeneous data quality. However, a less restrictive selection would not have seriously affected the results.

It is vital to avoid spurious correlations (or anti-correlations) between temperatures and intensities, because they would bias the resulting phase differences towards 0° or 180°. Such a correlation might already arise as a consequence of the inevitable data noise, if the same measurement is used to derive both, temperature and intensity. The solution consists in using independent data sets for both parameters, by extracting alternatively temperature or intensity from each measurement. The simplest scheme of toggling between individual temperature or intensity determinations would lead to aliassing problems by cutting the sampling frequency in half. Instead, we toggle between *pairs* of temperatures or intensities. We define the frequency coincidences between temperature and intensity spectral components within a tolerance dependent on the combined a-priori frequency errors. So, since the frequencies need not be exactly equal, the reference points used for phase definition become an issue, and therefore the phase comparison is done in the middle of the data window, as reported previously (e.g., Reisin and Scheer 1996a).

The amplitudes and phases of the corresponding temperature and intensity oscillations are used to derive Krassovsky's η. This is a complex number, with the modulus defined as the ratio of relative band intensity and temperature amplitudes, and the argument ϕ as the difference between the respective phases (positive, if intensity precedes temperature). Our band intensities are extrapolated from measured sample intensities using the rotational temperatures, which introduces some additional noise. To avoid this, we reconstruct band intensity spectral components indirectly from sample intensity spectral components, by making use of the analytical relation between both. At any rate, the direct use of band intensities also gave consistent results.

The linear theory by Hines and Tarasick (1987) of the observable effects of gravity waves on airglow emissions resulted in a remarkable separation between wave parameters and airglow chemistry. It is most

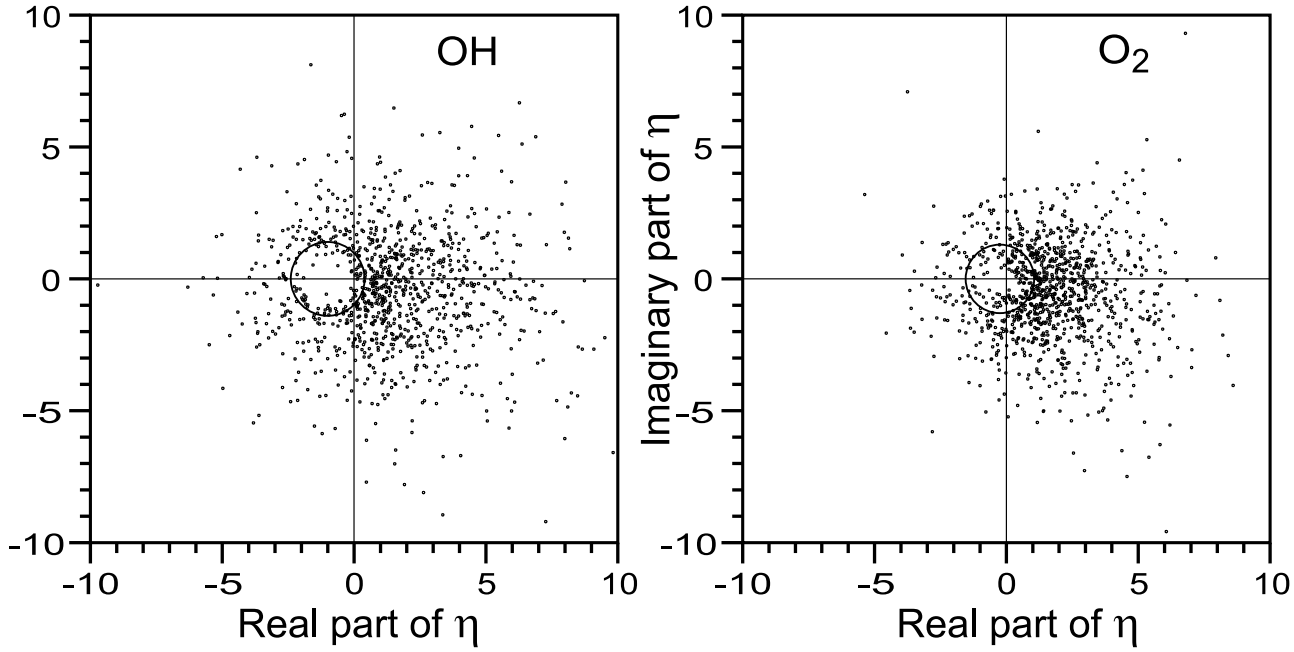

Fig. 1. Krassovsky's η derived from data 1997-2000. Circle marks area of noise signatures (see text).

clearly expressed in the following connection (derived from their equation 37) of λ_z with η: $\lambda_z \approx 22H/\eta_I$, where H is scale height, and $\eta_I = |\eta| \sin \phi$ is the imaginary part of η. λ_z is taken negative for downward phase propagation (i.e., upward energy propagation, in the normal case; see below). We maintain this notation consistent with Reisin and Scheer (1996a) while Hines and Tarasick (1987) used the opposite sign. This formula is valid for zenith observations, as ours.

RESULTS

Krassovsky's η

Figure 1 shows the resulting about 1000 wave signatures for each emission layer as values of η in the complex plane. In spite of data window overlap, the corresponding number of different wave events is not much smaller (about 700). That these points are due to gravity waves and not just due to measurement noise was tested by simulations.

By taking all the details of the real measurements into account the corresponding levels of photon counting noise were calculated. These data are processed with the same procedure as described above, for the real observations. The circles in Figure 1 mark the areas where 90% of these noise η values would fall. Fortunately, these areas are relatively small and are sufficiently separated from the maximum concentration of wave signatures. Therefore, discarding the points in these areas (as done for all the following analysis) is a simple and efficient way to discriminate against pure noise.

That the circles are shifted off the origin is another favourable consequence of the correction applied to spectra of sample intensities, as mentioned above. The low density of points close to the centers is an artifact due to the amplitude detection threshold for intensity oscillations.

The distributions of the points are centered at $|\eta| = 1.99 \pm 0.06$, for O_2, and $|\eta| = 1.69 \pm 0.07$, for OH, and for both emissions, $\phi = -17° \pm 2°$. These values signal the tendency towards the fourth quadrant also clearly visible in the figure. The predominant occupation of the first and fourth quadrants is in agreement with the theory of Hines and Tarasick (1987). However, there are also many points (15% for O_2, and 25% for OH) in the other quadrants, and only a part can be explained as outliers of the right-hand side population.

The scatter of the points is not due to statistical errors alone, as revealed by simulations of the effects of noise on wave signatures corresponding to given points in the η plain. Part of the variability may simply be due to the different wave parameters involved. Other possible factors are differences in mean atmospheric conditions like atomic oxygen profiles, wind shear, etc. That is, the situation is even more complex than in

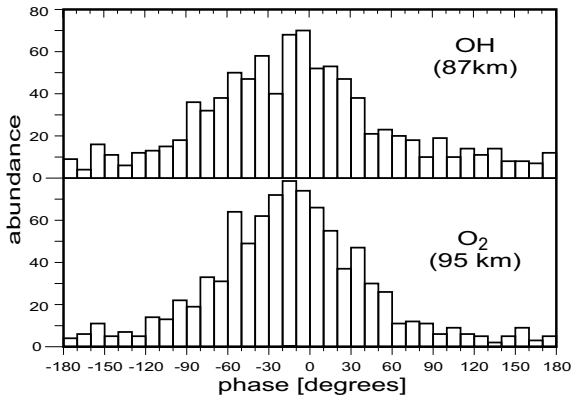

Fig. 2. Histogram of the phase of Krassovsky's η corresponding to data in Fig. 1

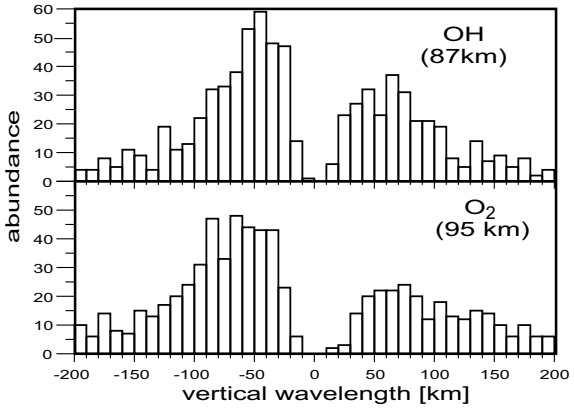

Fig. 3. Distribution of vertical wavelengths corresponding to Fig. 1

the tidal case with less dynamical degrees of freedom and smaller noise level (Reisin and Scheer 1996a).

Figure 2 shows the distribution of ϕ as a histogram with 10°bin size. This form of presenting the phase information contained in Figure 1 gives a clearer impression of the anisotropy. The wide distributions are clearly non-uniform, similar to normal distributions slightly shifted to negative phases. Evanescent or ducted waves correspond to $\phi \approx 0°$, according to the Hines and Tarasick theory. Here, they appear to be present only in a proportion consistent with the natural shape of the distributions, without any sign of an enhancement, or even prevalence.

There are very few cases near 180°, in striking contrast to literature claims of their frequent occurrence in experimental data. It is also more visible in Figure 2 that the number of cases with $|\phi| > 90°$ is higher for OH than for O_2. The cause of this difference is not related to noise level (which is similar, for both emissions), but it may be due to chemistry, as discussed by Tarasick and Shepherd (1992a, b) and Makhlouf et al. (1998).

Vertical Propagation

Histograms of λ_z derived via Hines' and Tarasick's relation are shown in Figure 3. The value of H used depends on mean temperature, and is typically 6 km. About 20% of the total number of cases are outside the range shown.

In addition to the generally expected downward phase propagation, there is a considerable number of waves with upward phase propagation. This is in general agreement with recent results by Gavrilov et al. (1997), using data from the MU radar at Shigaraki (34.9°N, 136.1°E). Wavelengths of 30 to 70 km, for OH, and 40 to 90 km, for O_2, are most frequently observed. This is similar for both directions of (phase) propagation.

The gap in the histogram for $\lambda_z \lesssim 20$ km is thought to be due to phase cancellation across the thickness of the airglow layers. Nearly all the waves described by Gavrilov et al. (1997) fall in this range. Our optical results are therefore complementary to those obtained with the MU radar.

Longer wavelengths are very sensitive to statistical errors, so that we cannot distinguish $\lambda_z \gtrsim 120$ km safely from evanescent or ducted waves, that do not propagate vertically. In order to more reliably quantify the proportions of upward, downward, and non-propagating waves, more simulations have been done to study the effects of statistical errors in detail. These simulations established three areas in the η plane that correspond to the 3 types of phase propagation ($\eta_I > 1$, $\eta_I < -1$, and $-1 < \eta_I < 1$, respectively), while estimating the amount of mutual leakage. From this we conclude, that about one third of the wave signatures correspond to non-propagating (evanescent or ducted) waves, for both emission layers. Of the propagating cases, 30% for O_2, and 39% for OH propagate upwards in phase.

In general, downward phase propagation means upward energy propagation. However, Gavrilov et al. (1997) discuss a situation when this is not so. In our view, the problem arises if the background wind

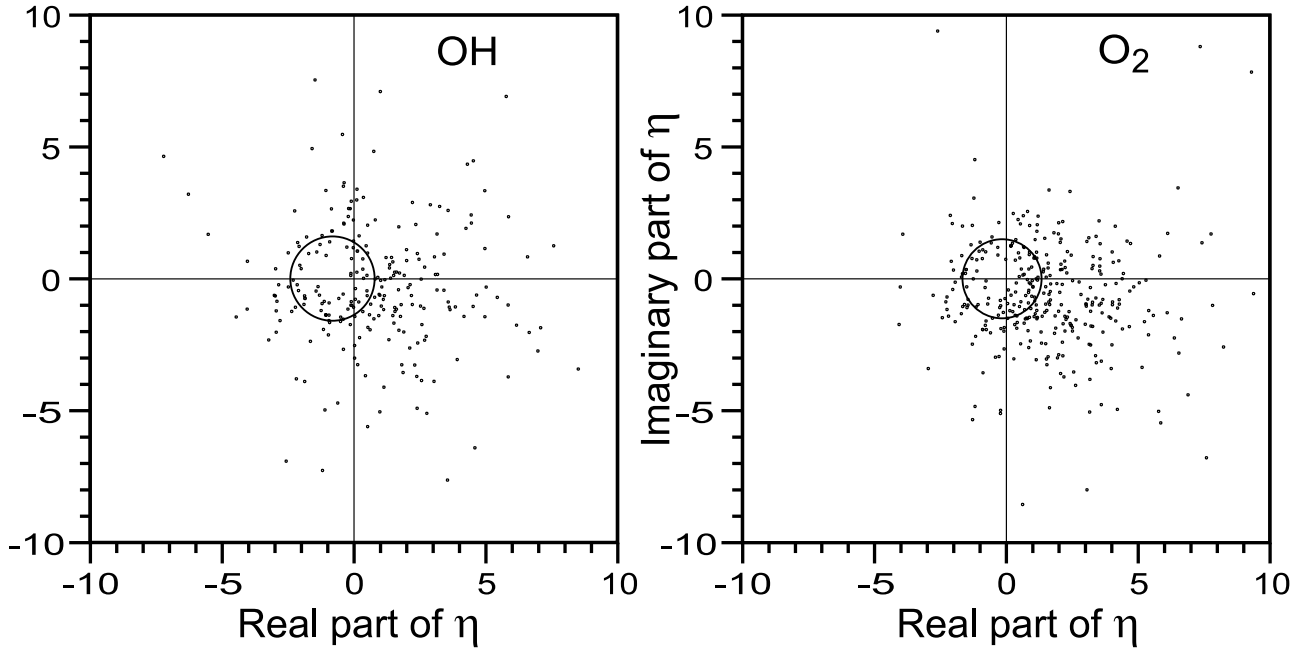

Fig. 4. Same as Fig. 1, but derived from data 1987, 1990, 1992.

component opposite to the direction of the horizontal wave propagation exceeds the intrinsic horizontal phase speed. Because of the inclined wave fronts, in this case the *observed* sense of vertical phase propagation changes sign to become equal to the energy propagation.

Such a situation is however not likely to seriously influence our statistical results. According to the approximate proportionality between horizontal phase speed and λ_z used by Swenson and Gardner (1998), phase speeds are at least 100 m/s for λ_z of 30 km and more, as in the majority of our results. Horizontal wind speeds are not likely to exceed 100 m/s, in the mesopause region. The chances that the Doppler effect changes the sign of the observed vertical phase propagation must therefore be small, taking also the relative azimuths between wave and wind into account. We would therefore expect an even smaller effect than the 5% estimated by Gavrilov et al. (1997), because of our greater λ_z.

We therefore conclude that 30% of the waves detected at 95 km, and nearly 40% of those at 87 km, have downward energy propagation. The smaller percentage at the upper height is consistent with reflection effects throughout the mesopause region. It is unlikely that such an appreciable downward wave flux be generated by local sources.

Comparison with Previous Results

As mentioned, the results discussed so far did not include our data taken before 1997. This is because of the different conditions under which they were obtained, as well as different sampling schemes. There have also been less restrictive selection criteria in the processing of the older data. It is however interesting to show some of these previous results here, for comparison. The η values corresponding to the data from Argentina in 1987 and 1992, and from Spain, in 1990, are shown in Figure 4 (Reisin and Scheer, 1996b). The 336 points for O_2 and 234 points for OH are based on 82 nights of observation with 19,000 sets of data. Despite the combination of data from different places and the other differences mentioned, the message of Figure 4 is essentially the same as the one contained in the more recent results described above.

CONCLUSIONS

The most important result is that our optical zenith observations can tell the difference between waves that propagate upward and those that propagate downward. In addition, it is clear that an appreciable part of the waves have upward phase propagation (about 30%, at 95 km, about 40%, at 87 km). If all the waves originate in the lower atmosphere, as is generally assumed, then reflection in or above the mesopause

region must play an important role. Such a conclusion is compatible with other recent airglow studies (e.g. Walterscheid et al., 2000), which are based on arguments completely different from ours.

There is only a very small contribution with $\phi \approx 180°$. Possibly these cases are just due to noise, or chemical effects, for OH. This is not an exception for a particular observing site, because we saw the same behaviour, in Spain. On the other hand, waves with $\phi \approx 0°$ are relatively frequent. Some may be evanescent, or very long wavelength, some may be ducted waves (Hines and Tarasick, 1994). However, our data show no special prevalence of those waves.

The vertical wavelengths are mostly greater than 20 km due to selectivity of the airglow method. Therefore, our results are complementary to radar and lidar observations.

Our recent results are consistent with those based on our older but much smaller data set.

ACKNOWLEDGEMENTS

The authors gratefully acknowledge the active support by the staff of Complejo Astronomico El Leoncito which has made the observational success of the recent years possible. This work was partially funded by CONICET and ANPCyT grants PMP PICT 0137, PIP 4554/96, and 07-00000-01818 / PICT '97-1818.

REFERENCES

Gavrilov, N. M., S. Fukao, T. Nakamura, and T. Tsuda, Statistical Analysis of Gravity Waves Observed with the Middle and Upper Atmosphere Radar in the Middle Atmosphere. 2. Waves Propagated in Different Directions, *J. Geophys. Res.* **102**, 13433-13440, 1997.

Hines C. O., and D. W. Tarasick, On the Detection and Utilization of Gravity Waves in Airglow Studies, *Planet. Space Sci.* **35**, 851- 866, 1987.

Hines, C. O., and D. W. Tarasick, Airglow response to vertically standing gravity waves, *Geophys. Res. Lett.* **21**, 2729-2732, 1994.

Reisin, E. R., and J. Scheer, Characteristics of Atmospheric Waves in the Tidal Period Range Derived from Zenith Observations of $O_2 b$(0-1) Atmospheric and OH(6-2) Airglow at Lower Mid-latitudes, *J. Geophys. Res.* **101**, 21223-21232, 1996a.

Reisin, E. R., and J. Scheer, Nuevos Avances en la Extracción de Parámetros de Ondas Atmosféricas Utilizando Temperaturas Rotacionales de las Emisiones de OH y O_2, *4a Conferencia Latinoamericana de Geofísica Espacial (COLAGE)*, Tucuman, April 22-26, 1996b.

Scheer, J., E. R. Reisin, J. P. Espy, M. Bittner, H.-H. Graef, D. Offermann, P. P. Ammosov, and V. M. Ignatyev, Large-scale Structures in Hydroxyl Rotational Temperatures during DYANA, *J. Atmos. Terr. Phys.* **56**, 1701-1715, 1994.

Scheer, J., and E. R. Reisin, Unusually Low Airglow Intensities in the Southern Hemisphere Midlatitude Mesopause Region, *Earth Planets and Space* **52**, 261-266, 2000.

Scheer, J., and E. R. Reisin, Refinements of a Classical Technique of Airglow Spectroscopy, *Adv. Space Res.*, in press, 2001.

Swenson, G. R., and C. S. Gardner, Analytical Models for the Responses of the Mesospheric OH^* and Na to Atmospheric Gravity Waves, *J. Geophys. Res.* **103**, 6271-6294, 1998.

Takahashi, H., P. P. Batista, R. A. Buriti, D. Gobbi, T. Nakamura, T. Tsuda, and S. Fukao, Response of the Airglow OH Emission, Temperature and Mesopause Wind to the Atmospheric Wave Propagation over Shigaraki, Japan, *Earth Planets and Space* **51**, 863-875, 1999.

Tarasick, D. W., and G. G. Shepherd, Effects of Gravity Waves on Complex Airglow Chemistries. 1. $O_2(b^1\Sigma^+{}_g)$ Emission, *J. Geophys. Res.* **97**, 3185-3193, 1992a.

Tarasick, D. W., and G. G. Shepherd, Effects of Gravity Waves on Complex Airglow Chemistries. 2. OH Emission, *J. Geophys. Res.* **97**, 3195- 3208, 1992b.

Walterscheid, R. L., J. H. Hecht, R. A. Vincent, I. M. Reid, J. Woithe, and M. P. Hickey, Analysis and Interpretation of Airglow and Radar Observations of Quasi-Monochromatic Gravity Waves in the Upper Mesosphere and Lower Thermosphere over Adelaide, Australia (35°S, 138°E), *J. Atmos. Solar-Terr. Phys.* **61**, 461-478, 1999.

Walterscheid, R. L., J. H. Hecht, F. T. Djuth, and C. A. Tepley, Evidence of reflection of a long-period gravity wave in observations of the nightglow over Arecibo on May 8-9, 1989, *J. Geophys. Res.* **105**, 6927-6934, 2000.